Controlling Structure and Reactivity in Cationic Solid–State Molecular OrganoMetallic (SMOM) Systems using Anion Templating.

Alasdair I. McKay,[†] Antonio J. Martínez-Martínez,[†] Hannah J. Griffiths,[†] Nicholas H. Rees,[†] Jordan B. Waters,[†] Andrew S. Weller,[†,*] Tobias Krämer,[‡§] Stuart A. Macgregor[‡,*]

[†]Department of Chemistry, University of Oxford, Mansfield Road, Oxford, OX1 3TA, U.K.

[‡]Institute of Chemical Sciences, Heriot-Watt University, Edinburgh, EH14 4AS, U.K.

§Current address: Department of Chemistry, Maynooth University, Maynooth, Co. Kildare, Ireland.

ABSTRACT: The role that the supporting anion has on the stability, structure and catalytic performance, in Solid-state Molecular OrganoMetallic systems (SMOM) based upon $[Rh(Cy_2PCH_2CH_2PCy_2)(\eta^2\eta^2\text{-NBD})][BAr^X{}_4]$, **[1-NBD][BAr^X$_4$]**, is reported (X = Cl, F, H; NBD = norbornadiene). The tetra–aryl borate anion is systematically varied at the 3,5–position, Ar^X= 3,5-$X_2C_6H_3$, and the stability and structure in the solid–state compared with the previously reported **[1-NBD][BAr^{CF_3}$_4$]** complex. Single crystal X-ray crystallography shows that the three complexes have different packing motifs, in which the cation sits on the shared face of two parallelepipeds for **[1-NBD][BAr^{Cl}$_4$]**, is surrounded by eight anions in gyrobifastigium arrangement for **[1-NBD][BAr^F$_4$]**, or the six anions show an octahedral cage arrangement in **[1-NBD][BAr^H$_4$]**, similar to **[1-NBD][BAr^{CF_3}$_4$]**. C-X···X-C contacts, commonly encountered in crystal–engineering, are suggested to be important in determining structure. Addition of H_2 in a solid/gas reaction affords the resulting σ–alkane complexes, $[Rh(Cy_2PCH_2CH_2PCy_2)(\eta^2\eta^2\text{-NBA})][BAr^X{}_4]$ **[1-NBA][BAr^X$_4$]** (NBA = norbornane), which can then proceed to lose the alkane and form the zwitterionic, anion coordinated, complexes. The relative rates at which hydrogenation and then decomposition of σ–alkane complexes proceed are shown to be anion dependent. **[BAr^{CF_3}$_4$]$^-$** promotes fast hydrogenation and an indefinitely stable σ–alkane complex. With **[BAr^H$_4$]$^-$** hydrogenation is slow and the σ–alkane complex so unstable it is not observed. **[BAr^{Cl}$_4$]$^-$** and **[BAr^F$_4$]$^-$** promote intermediate reactivity profiles, and for **[BAr^{Cl}$_4$]$^-$** a single–crystal to single–crystal hydrogenation results in **[1-NBA][BAr^{Cl}$_4$]**. The molecular structure derived from X-ray diffraction reveals a σ–alkane complex in which the NBA fragment is bound through two *exo* Rh···H–C interactions – different from the *endo* selective binding observed with **[1-NBA][BAr^{CF_3}$_4$]**. Periodic DFT calculations demonstrate that this selectivity is driven by the microenvironment dictated by the surrounding anions. **[1-NBA][BAr^X$_4$]** are catalysts for gas/solid 1–butene isomerization (298 K, 1 atm) and their activity can be directly correlated to the stability of the σ–alkane complex compared to the anion–coordinated decomposition products.

1. INTRODUCTION

The functionalization of alkanes via C–H activation to produce commodity and fine chemicals or new materials is of considerable contemporary interest.[1-4] σ-Alkane complexes, in which the C–H bond engages in a 3–center 2–electron interaction with the metal center,[5] have long been recognised as key intermediates in C–H activation processes that occur by an inner–sphere mechansim.[6-12] σ-Alkane complexes are also of interest in terms of their challenging, but fundamentally important, coordination chemistry. The strong non-polar C–H bond in alkanes, combined with the steric hindrance of proximal groups, mean that alkanes are very poor ligands, typically binding to metal centers with bond enthalpies of ~60 kJ mol^{-1} or less.[9,13-14] The characterization of σ-alkane complexes has been generally limited to very low–temperature, in situ, solution–based spectroscopic studies, e.g. TRIR or NMR spectroscopy, either by photogeneration of a coordinatively unsaturated metal center in a solvent that also acts as a proligand,[15-18] or protonation of a metal-alkyl complex with a strong acid;[19-20] for example $[Re(HEB)(CO)_2(CypH)][Al\{OC(CF_3)_3\}_4]$ (HEB = η^6–hexaethylbenzene, Cyp = cyclopentyl),[21] or $[Rh(PONOP)(H_4C)][BAr^{CF_3}{}_4]$ (PONOP = (2,6-^{t}Bu$_2$PO)$_2$C$_5$H$_3$N, Ar^{CF_3} = 3,5-$(CF_3)_2(C_6H_3)$) respectively. Although these elegant techniques allow for the direct observation of σ-alkane complexes by NMR spectroscopy, these are generated in low absolute quantities (e.g., 1–20 mg) and are relatively short–lived, e.g. half–lives of less than 90 minutes at 212 K. This makes such routes less than optimal for the generation of materials suitable for structural elucidation by single–crystal X-ray diffraction techniques, or onward reactivity studies. We recently reported an alternative route to form σ-alkane complexes directly in the solid–state, by solid/gas single–crystal to single–crystal transformation[22-23] thereby enabling the structure of the product to be determined by single–crystal X-ray diffraction and solid–state NMR techniques. It also allows for structures to be further interrogated by periodic DFT computational analysis. Exemplifying this approach, addition of H_2 to the diene precursor $[Rh(Cy_2PCH_2CH_2PCy_2)(\eta^2\eta^2\text{-NBD})][BAr^{CF_3}{}_4]$, **[1-NBD][BAr^{CF_3}$_4$]**, (NBD = norbornadiene) affords $[Rh(Cy_2PCH_2CH_2PCy_2)(\eta^2\eta^2\text{-NBA})][BAr^{CF_3}{}_4]$ (**[1-NBA][BAr^{CF_3}$_4$]**, NBA = norbornane) in essentially quantitative yield (Figure 1A),[24] in which a saturated NBA fragment interacts with the Rh–center through two *endo*–C–H···Rh 3c–2e interactions. This complex is remarkably stable in the solid–state

(months at 298 K under Ar) with respect to NBA loss and formation of the $[BAr^{CF_3}{}_4]^-$ coordinated zwitterion, $[Rh(Cy_2PCH_2CH_2PCy_2)\{(\eta^6\text{-}C_6H_3(CF_3)_2)BAr^{CF_3}{}_3\}]$, **[1-BAr$^{CF_3}{}_4$]**. With other substituents on phosphorus stability is significantly reduced. For example when R = cyclopentyl (Cyp) a lifetime of 96 hours is measured,[25] while when R = ^{i}Bu stability at 298 K is limited to only a few hours.[26] Stability is enhanced at lower temperatures, allowing for characterization by single–crystal X-ray diffraction techniques at 150 K. We speculate that the general stability in the solid–state of σ–alkane complexes such as **[1-NBA][BAr$^{CF_3}{}_4$]**, and its analogues, originates from an octahedral cavity defined by the $[BAr^{CF_3}{}_4]^-$ anions (Figures 1B and C), which permits the hydrogenation of the alkene to occur without loss of crystallinity, trapping the resultant alkane. These anions thus provide a microenviroment that allows for transformations within a crystalline "molecular flask".[27] We describe these exceptionally well–defined systems as Solid–state Molecular Organometallics (SMOM) in reference to related, and well–developed, Supported Organometallic Catalysts (SOMC)[28] and Single–Site Heterogeneous Catalysts (SSHC),[29] and like these systems they support transformations such as C–H activation[30] and catalysis, e.g. solid/gas alkene isomerization.[31]

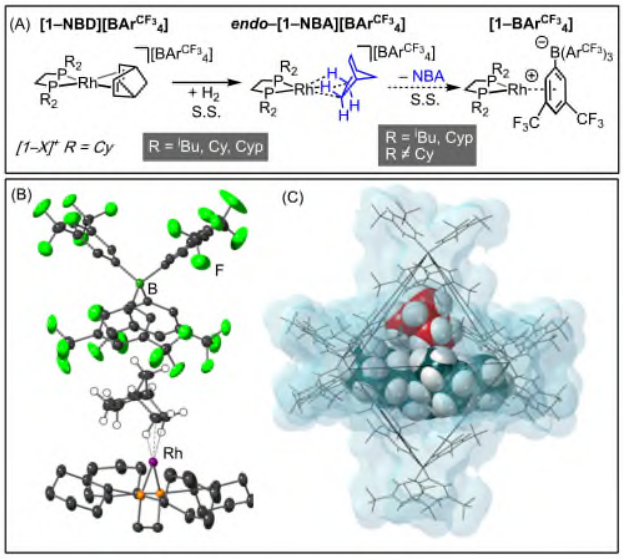

Figure 1. (A) Synthesis of σ-alkane complexes in the solid-state; (B) Solid-state structure of **[1-NBA][BAr$^{CF_3}{}_4$]**; (C) Packing of anions around a single cation (van der Waals radii).

The precise factors governing the variation of relative stabilities of these complexes on changing the phosphine ligand are not fully resolved, although we have noted that the steric profile appears to be important,[25] while a number of weak C-H···F-C hydrogen bonds in the extended lattice may contribute to kinetic and/or thermodynamic stability.[24] In this contribution we concentrate on the role that the supporting anion has on the stability, structure and catalytic performance, of SMOM–catalysts based upon **[1–NBA]$^+$**, in which the anion is systematically varied (Scheme 1) using various tetra–aryl borates in which substitution at the 3,5–position is changed. Although anion effects are well–documented in homogenous organometallic chemistry and catalysis,[32-33] their influence in the solid–state with regard to single–crystal to single–crystal synthesis and catalysis is considerably less–well developed.[34-37]

Scheme 1. SMOM–systems studied in this contribution

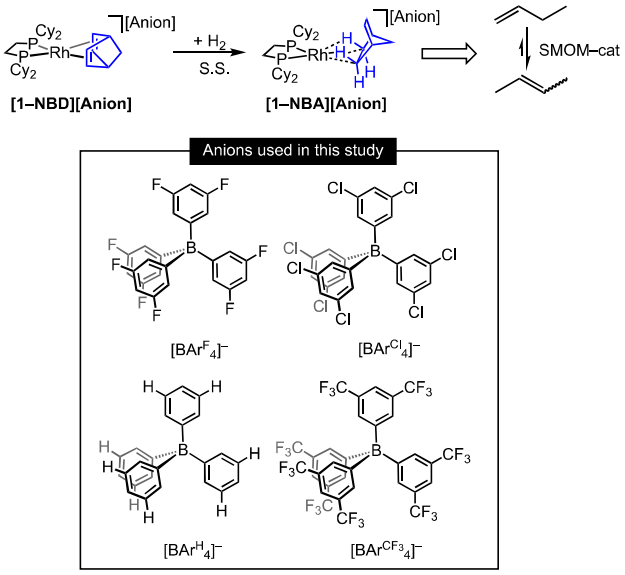

2. RESULTS AND DISCUSSION

2.1 Variation of the Borate Anion in the 3,5 positions: Effects on Structure. The new precursor complexes **[1-NBD][BAr$^{Cl}{}_4$]** (Ar^{Cl} = 3,5–$Cl_2C_6H_3$), **[1-NBD][BAr$^F{}_4$]** (Ar^F = 3,5–$F_2C_6H_3$) and **[1-NBD][BAr$^H{}_4$]** (Ar^H = C_6H_5) were synthesized by addition of the respective sodium borate salt to a dichloromethane solution of $[RhCl(Cy_2PCH_2CH_2PCy_2)]_2$ in the presence of excess NBD (Scheme 2).

Scheme 2. Synthesis of NBD Precursor Complexes

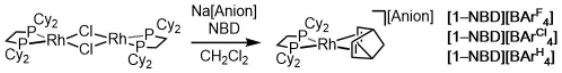

Solution NMR data are fully consistent with their formulation (Supporting Materials) being similar to previously reported examples.[24,38] Orange single–crystals suitable for single-crystal X-ray diffraction could be grown from CH_2Cl_2/pentane solvent mixtures, and the resulting solid–state structures determined are shown in Figure 2. The effect of the anions on the solid–state structure is signaled by the three complexes crystallizing in different space groups: **[1-NBD][BAr$^{Cl}{}_4$]** *P*-1 (Z' = 1), **[1-NBD][BAr$^F{}_4$]** *Fdd2* (Z' = 0.5) and **[1-NBD][BAr$^H{}_4$]** *Pbca* (Z' = 1). The cations show unremarkable structural metrics, being very similar to that of the parent complex **[1-NBD][BAr$^{CF_3}{}_4$]**. However, consideration of the packing of the anions in the lattice shows a dramatic difference between all three. For **[1-NBD][BAr$^{Cl}{}_4$]** the cation sits on the shared face of two parallelepipeds, but there is no crystallographically imposed symmetry. In **[1-NBD][BAr$^F{}_4$]** the cation is surrounded by eight anions which adopt a gyrobifastigium arrangement (two face-sharing trigonal prisms), and sits on a special position generating C_2 symmetry. For **[1-NBD][BAr$^H{}_4$]** each cation is surrounded by six anions in an octahedral cage arrangement, similar to that in **[1-NBD][BAr$^{CF_3}{}_4$]** (*P*–1, *Z* = 2).[24] However, unlike in **[1-NBD][BAr$^{CF_3}{}_4$]** where the {Rh(NBD)} points towards the apical borate and is flanked by two of its Ar^{CF_3} groups, the NBD ligand in **[1-NBD][BAr$^H{}_4$]** points to an edge of the octahedron (Figures 1B and 2C). This is a consequence of the different local orientation of the

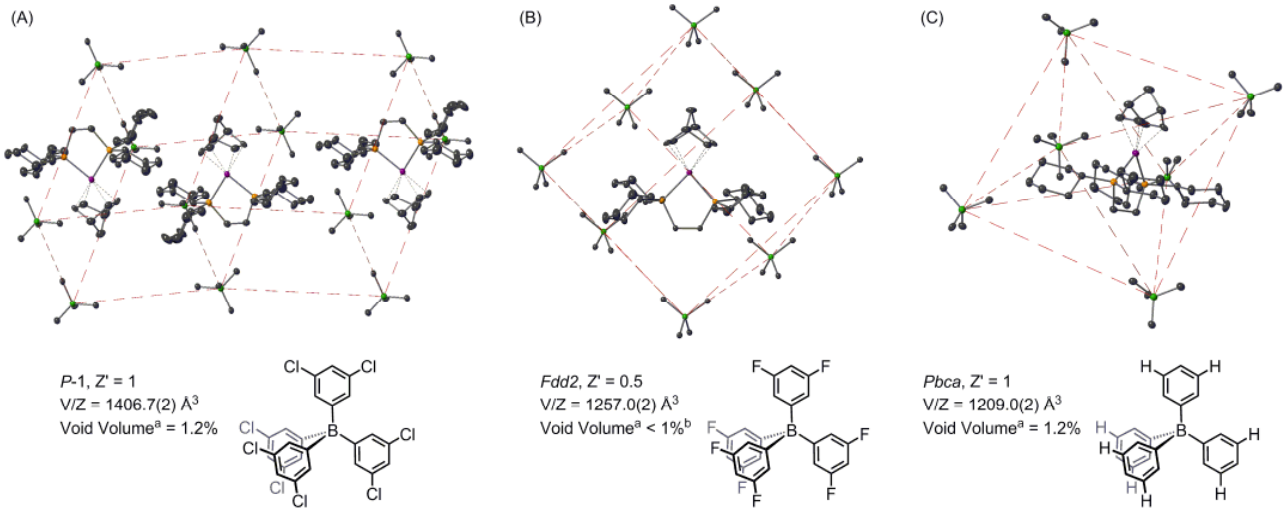

Figure 2. Extended solid–state structures of (A) **[1-NBD][BAr$^{Cl}_4$]**; (B) **[1-NBD][BAr$^{F}_4$]**; (C) **[1-NBD][BAr$^{H}_4$]**. Ar^X groups omitted. [a] Solvent accessible voids calculated by PLATON,[39] expressed as a percentage of the unit cell volume. [b] No solvent accessible voids were identified.

$[BAr^{H}_4]^-$ anions compared to $[BAr^{CF_3}_4]^-$ in which aryl groups of the former penetrate the cavity of the octahedron (Supporting Materials), and for which the volume is also smaller (average cross–cage B···B distances of 16.9 and 18.8 Å respectively).

The extended solid-state structures of both **[1-NBD][BAr$^{F}_4$]** and **[1-NBD][BAr$^{Cl}_4$]** display interanion contacts. In **[1-NBD][BAr$^{F}_4$]**, the F1···H27 distance of 2.465(2) Å (Figure 3B) lies well within the combined van der Waals radii of F and H (2.66 Å)[40] being comparable to that reported in the solid-state structure of fluorobenzene (2.47 Å).[41] The C27–H27···F1 angle is essentially linear, 174.4(2)º. For **[1-NBD][BAr$^{Cl}_4$]** a number of interanion chlorine···chlorine contacts (Cl1···Cl6 3.412(1) Å, Cl1···Cl8 3.575(1) Å, Figure 3A) also lie within the combined van der Waals radii (3.64 Å),[40] and are arranged close to 90º [100.97(9) and 80.35(8)º respectively]. These are best described as Type II C-X···X-C contacts,[42] which are similar to those observed in the solid-state structure of 1,3-dichlorobenzene.[43] These types of halogen···hydrogen[44] and halogen···halogen[45] contacts have been widely utilized in crystal engineering.[46] Given that these two anions are, essentially isosteric, these interactions – albeit weak – clearly influence the extended packing motif in the lattice. Long interanion contacts are observed in the solid-state structure of **[1-NBD][BAr$^{CF_3}_4$]** (F4···F8 2.913(3) Å, F17···F220 2.924(6) Å), which lie within error of the combined van der Waals radii (2.92 Å).[40] There are no interanion contacts in **[1-NBD][BAr$^{H}_4$]** that lie within the sum of van der Waals radii.

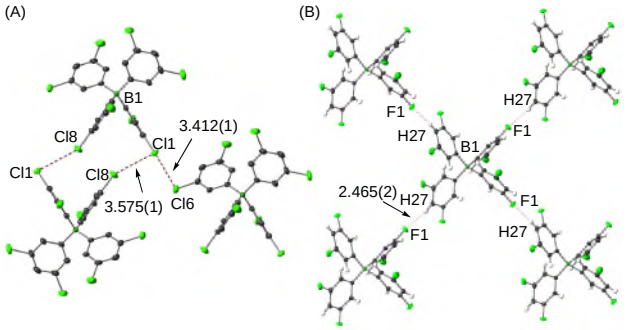

Figure 3. Interanion interactions in the solid-state structures of (A) **[1-NBD][BAr$^{Cl}_4$]**; (B) **[1-NBD][BAr$^{F}_4$]**.

These new NBD complexes have been studied by solid–state NMR (SSNMR) techniques at 294 K. The $^{31}P\{^1H\}$ SSNMR spectrum of **[1-NBD][BAr$^{Cl}_4$]** features two distinct but closely spaced phosphine environments [δ 64.7, *J*(RhP) = 145 Hz; δ 63.0, *J*(RhP) = 147 Hz]. Similarly for **[1-NBD][BAr$^{H}_4$]** two phosphine environments are observed [δ 75.8, *J*(RhP) = 134 Hz; δ 64.8, *J*(RhP) = 132 Hz]. The observation of two ^{31}P environments is consistent with the solid–state structures that have crystallographically non–equivalent phosphines. In contrast the $^{31}P\{^1H\}$ SSNMR spectrum of **[1-NBD][BAr$^{F}_4$]** displays a single, broad, ^{31}P environment at δ 70.9, consistent with the C_2 symmetry observed in its solid-state structure, although coupling to ^{103}Rh was not resolved. These features are mirrored in the corresponding $^{13}C\{^1H\}$ SSNMR spectra. **[1-NBD][BAr$^{Cl}_4$]** and **[1-NBD][BAr$^{H}_4$]** each feature six signals[47] between δ 90 and 50, which are assigned to the NBD fragment; while the $^{13}C\{^1H\}$ SSNMR spectrum of **[1-NBD][BAr$^{F}_4$]** displays four distinct signals assigned to the NBD fragment under crystallographic C_2 symmetry.

2.2 Reactivity of [1-NBD][BAr$^X_4$] (X = Cl, F, H) with H_2 in the solid–state as studied by NMR spectroscopy. With the complexes **[1-NBD][BAr$^X_4$]** in hand their solid/gas reactivity with H_2 was studied with respect to changing the anion–identity, and compared against **[1-NBD][BAr$^{CF_3}_4$]**. Finely powdered single crystals of **[1-NBD][BAr$^X_4$]** were exposed to H_2 (1 bar, 298 K) for various periods of time, H_2 was then removed under vacuum, dichloromethane was added by vacuum transfer and the sample warmed to 298 K. The extent of hydrogenation was determined by comparing the relative integrals in the $^{31}P\{^1H\}$ NMR spectrum of the starting material and zwitterionic **[1-BAr$^X_4$]** (Figure 4A). Complexes **[1-BAr$^X_4$]** have been independently prepared and characterized (Supporting Materials).[48] This methodology only indirectly signals the formation of a σ–alkane complex, i.e. **[1-NBA][BAr$^X_4$]**, as the alkane would be rapidly displaced by the anion on solvation.[24] However, it does allow for the expedient measurement of the relative rates of hydrogenation in the solid–state.

These data reveal the rate of NBD hydrogenation to be anion–dependent, with replacement of the 3,5-$(CF_3)_2$ substituents on the borate resulting in significantly slower reactions. For **[1-NBD][BAr$^{F}_4$]** hydrogenation of the NBD ligand is only complete after ~24 h. By contrast **[1-NBD][BAr$^{Cl}_4$]** and **[1-NBD][BAr$^{H}_4$]** are both hydrogenated in 2 hours, although this is still considerably slower than for **[1-NBD][BAr$^{CF3}_4$]** for which a maximum time of 15 minutes is obtained (first measured point). These different rates of hydrogenation are also signaled by color changes to the crystalline material. While orange microcrystalline **[1-NBD][BAr$^{Cl}_4$]** and **[1-NBD][BAr$^{F}_4$]** undergo little immediate color change, over longer times (3 hours) the color of the powder changed to yellow which is characteristic of zwitterion formation. For **[1-NBD][BAr$^{H}_4$]** this color change was more rapid (10 minutes).

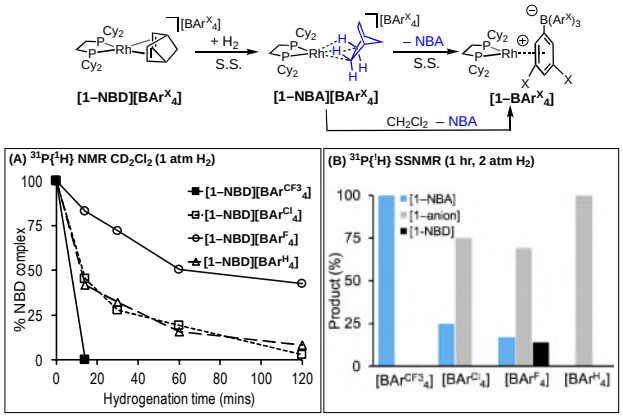

Figure 4. (A) Temporal evolution of H_2 addition (1 bar, 298 K, first 2 hours) to **[1–NBD][BAr$^{X}_4$]** (X = Cl, F, H, CF_3) as measured by the formation of **[1-BAr$^{X}_4$]** in CD_2Cl_2 solution;[48] (B) Selectivity of **[1–NBA][BAr$^{X}_4$]** formation after H_2 addition (2 bar, 298 K, 1 hour) as measured by $^{31}P\{^1H\}$ SSNMR at 158 K.

Following the hydrogenation in the solid–state (2 bar, 1 h, 298 K)[49] of **[1-NBD][BAr$^{Cl}_4$]** by $^{31}P\{^1H\}$ SSNMR spectroscopy (measured at 158 K to slow decomposition – vide infra) revealed complete consumption of the starting material to form an intermediate species [δ 102.7, *J*(RhP) ≈ 180 Hz; δ 97.2, *J*(RhP) ≈ 198 Hz]. These data are similar to those reported for **[1-NBA][BAr$^{CF3}_4$]** [δ ~110, *J*(RhP) ≈ 207 and 216 Hz] (Figure 4B).[24] The $^{13}C\{^1H\}$ SSNMR spectrum confirmed that hydrogenation of the alkene had occurred, with the disappearance of diagnostic signals at δ 88.4, 87.4, 80.3 and 79.4 assigned to alkene in the starting material. These data signal the formation of a σ–alkane complex **[1-NBA][BAr$^{Cl}_4$]**. The $^{31}P\{^1H\}$ SSNMR resonances were accompanied by a broad signal centered at δ 86 (relative ratio 25:75), assigned to the amorphous decomposition product **[1-BAr$^{Cl}_4$]** which has been independently synthesized and crystallographically characterized, and is similar to that reported for [Rh(^{i}Bu$_2$PCH$_2$CH$_2$P^{i}Bu$_2$){(η^6-C$_6$H$_3$Cl$_2$)BAr$^{Cl}_3$}].[50,38] We have not observed **[1-NBA][BAr$^{Cl}_4$]** free of zwitterion product, however low temperatures halt onward decomposition. Complete decomposition of **[1-NBA][BAr$^{Cl}_4$]** occurs in 7 h at 294 K. This stability of **[1-NBA][BAr$^{Cl}_4$]** is notable considering the room temperature hydrogenation of microcrystalline [Rh(^{i}Bu$_2$PCH$_2$CH$_2$P^{i}Bu$_2$)(η^{2}η^2-NBD)][BAr$^{Cl}_4$] affords [Rh(^{i}Bu$_2$PCH$_2$CH$_2$P^{i}Bu$_2$)(η^6-C$_6$H$_3$Cl$_2$)BAr$^{Cl}_3$] quantitatively in 10 minutes and no intermediate alkane sigma complex is observed,[38] reflecting the influence of the phosphine steric–profile on σ–complex stability.

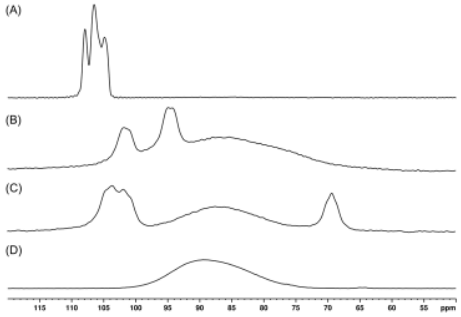

Figure 5. $^{31}P\{^1H\}$ SSNMR spectra (158 K) of H_2 addition (2 bar, 298 K, 1 hour) to powdered crystalline **[1-NBD][BAr$^{X}_4$]**. (A) **[1-NBD][BAr$^{CF3}_4$]**; (B) **[1-NBD][BAr$^{Cl}_4$]**; (C) **[1-NBD][BAr$^{F}_4$]**; (D) **[1-NBD][BAr$^{H}_4$]**.

Although hydrogenation of **[1-NBD][BAr$^{H}_4$]** occurs at the same rate as **[1-NBA][BAr$^{Cl}_4$]** (Figure 4A) an intermediate alkane complex is not observed. The $^{31}P\{^1H\}$ SSNMR spectrum (158 K, Figure 5D) of hydrogenated microcrystalline **[1-NBD][BAr$^{H}_4$]** (2 bar, 1 hour, 298 K), features a single very broad resonance centered at δ 89.0, which is assigned to the amorphous zwitterionic decomposition product **[1-BAr$^{H}_4$]**, which has been independently prepared (Supporting Materials). Zwitterionic complexes of Rh(PR$_3$)$_2${(η^6-C$_6$H$_5$)BAr$^{H}_3$}, and related complexes, are well known.[51-55] No signals were observed that could be assigned to a sigma–alkane complex. For **[1-NBD][BAr$^{F}_4$]**, after hydrogenation for 1 hour, two broad closely spaced downfield doublets where observed [δ 105.1, *J*(RhP) ~ 180 Hz; δ 102.2, *J*(RhP) ~ 190 Hz] that are assigned to the σ-alkane complex **[1-NBA][BAr$^{F}_4$]**. However, a very broad resonance [δ 89.3, ca. 69%] also dominates that is assigned to an amorphous phase of zwitterionic **[1-BAr$^{F}_4$]**, in addition to starting material (14%). **[1-BAr$^{F}_4$]** has been independently synthesized and crystallographically characterized (Figure 6 and Supporting Materials) and presents a rare example of this anion coordinating with a metal center in an η^6–motif. Structures showing κ^1–[56] and κ^2–[57] F···M interactions with the [B(C$_6$F$_5$)$_4$]$^-$ are known. These data are consistent with the slower rate of hydrogenation in the solid–state for **[1-NBD][BAr$^{F}_4$]**, but also

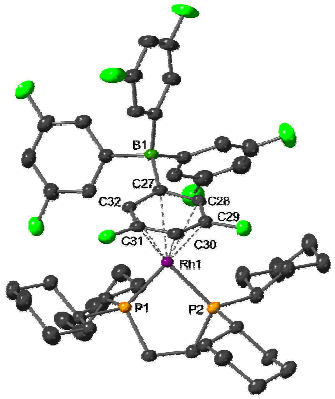

Figure 6. Solid-state structure of **[1-BAr$^{F}_4$]**. Displacement ellipsoids are shown at 50% probability level, second molecule in the asymmetric unit and hydrogen atoms omitted for clarity. Selected bond distances (Å): Rh1-P1 2.2631(5), Rh1-P2 2.2449(5), Rh1-C27 2.4604(18), Rh1-C28 2.3423(18), Rh1-C29 2.2802(18), Rh1-C30 2.3908(18), Rh1-C31 2.3194(18), Rh1-C32 2.3185(18).

that the stability of **[1-NBA][BAr$^{F}_{4}$]** with respect to zwitterion formation must be sufficient to allow for its observation, albeit not as the major species after 1 hour. The broad signals observed in the $^{31}P\{^{1}H\}$ SSNMR that are assigned to amorphous phases of these zwitterionic complexes have been noted previously for [Rh(^{i}Pr$_2$PCH$_2$CH$_2$P^{i}Pr$_2$)(η^6-C$_6$H$_3$(CF$_3$)$_2$)BAr$^{CF_3}_{3}$] which, interestingly, undergoes a phase change at 323 K to give crystalline material, resulting in sharper signals.[24] We have not investigated whether this occurs for **[1-BAr$^{X}_{4}$]** X = F, Cl, H.

We have previously used $^{1}H/^{13}C$ FSLG-HETCOR SSNMR experiments[58] to indirectly detect Rh···H–C interactions in σ–alkane complexes.[24-25,59] The HETCOR spectrum (158 K) of **[1-NBA][BAr$^{Cl}_{4}$]** (as prepared as a mixture with **[1–BAr$^{Cl}_{4}$]**) features a high–field ^{1}H cross–peak (δ –3.1) which correlates to a partially obscured ^{13}C signal at δ 25 assigned to the NBA carbon atoms involved in the 3c-2e interaction (Supporting Materials). We did not observe a distinctive cross peak for the bridge methylene group in NBA to high–field shifted proton signals. This is different to that in **[1-NBA][BAr$^{CF_3}_{4}$]** in which a ^{13}C signal at ~ δ 44 correlates to a high–field shifted peak in the ^{1}H NMR projection, that is due to these protons experiencing ring current shielding from the proximal 3,5–(CF$_3$)$_2$C$_6$H$_3$ groups in the lattice.[24,59] This suggests a different structure for **[1-NBA][BAr$^{Cl}_{4}$]** (vide infra). We were not successful in obtaining a meaningful HETCOR spectrum of **[1-NBA][BAr$^{F}_{4}$]**.

These data, combined, show that the **[BAr$^{CF_3}_{4}$]$^-$** anion promotes fast hydrogenation of the NBD precursor to form a stable alkane complex, as already reported.[24] In comparison, although [**1-NBD][BAr$^{H}_{4}$]** shares a similar solid–state packing environment, hydrogenation is significantly slower while anion coordination and alkane loss occurs at a comparable, likely faster, rate that means that the intermediate σ–alkane complex is not seen. For [**1-NBD][BAr$^{Cl}_{4}$]** and **[1-NBD][BAr$^{F}_{4}$]** the situation is more finely balanced. The motif present in **[1-NBD][BAr$^{F}_{4}$]**, with C-H···F interactions, clearly inhibits the hydrogenation of the coordinated NBD; while the relative lack of stability of the corresponding σ–alkane complex, **[1-NBA][BAr$^{F}_{4}$]**, with respect to the zwitterion **[1-BAr$^{F}_{4}$]**, means that this complex is never observed as the major species. For **[1-NBA][BAr$^{Cl}_{4}$]** this situation is balanced more in favor of the alkane complex over starting material. Although rate of hydrogenation is essentially the same as for **[1-NBD][BAr$^{H}_{4}$]**, the alkane complex is persistent and can be observed alongside amorphous **[1–BAr$^{Cl}_{4}$]**. These observations indicate that the fluorous–CF_3 groups may facilitate H_2 transport through the non–porous crystal[35,60-63] and/or permit rearrangement of the NBD fragment necessary to promote hydrogenation and formation of a σ–alkane complex, while retaining the same microenvironment of [BAr$^{CF_3}_{4}$]$^-$ anions to allow for subsequent observation of the σ–alkane complex.

2.3 Characterization of a σ–alkane complex by single–crystal X-ray Crystallography. The temporal profile of hydrogenation coupled with the relative lifetime of the σ–alkane complex encouraged a single–crystal to single–crystal study of the hydrogenation of **[1-NBD][BAr$^{Cl}_{4}$]**. H_2 was added to crystalline material (2 bar, 298 K) and a selected single–crystal rapidly transferred to the cryostream (150 K) of an X-ray diffractometer. This procedure was repeated a number of times to optimize the hydrogenation time (30 minutes) to obtain the highest–quality structure. Under these temporal conditions (cf Figure 4) the best solution still had ~7% of **[1-NBD][BAr$^{Cl}_{4}$]** in the lattice, that could be adequately accounted for at this partial occupancy. Longer reaction times (> 1 h) afforded solids that had lost long–range order (i.e. Figure 5B). The solid-state structure of **[1-NBA][BAr$^{Cl}_{4}$]** is shown in Figure 7A. This single-crystal to single-crystal transformation proceeds without a change in space group (*P*–1) or the overall structural motif of the anion–packing. The structural model is consistent with the coordination of norbornane with the metal center through two, η^2, 3c–2e Rh···H–C bonds. The Rh-C27/C28 distances [2.387(5) and 2.378(5) Å respectively] are the same, within error, as those reported for **[1-NBA][BAr$^{CF_3}_{4}$]** [2.389(3) and 2.400(3) Å].[24] The C27–C28 and C30–C31 distances [1.561(7) and 1.548(9) Å] confirm the hydrogenation of the diene to afford an alkane. The Rh–P distances are shorter than in the precursor NBD complex [e.g. Rh–P1, 2.2095(11), cf. 2.3008(6) Å], and reflect the low *trans* influence of the sigma alkane interaction.

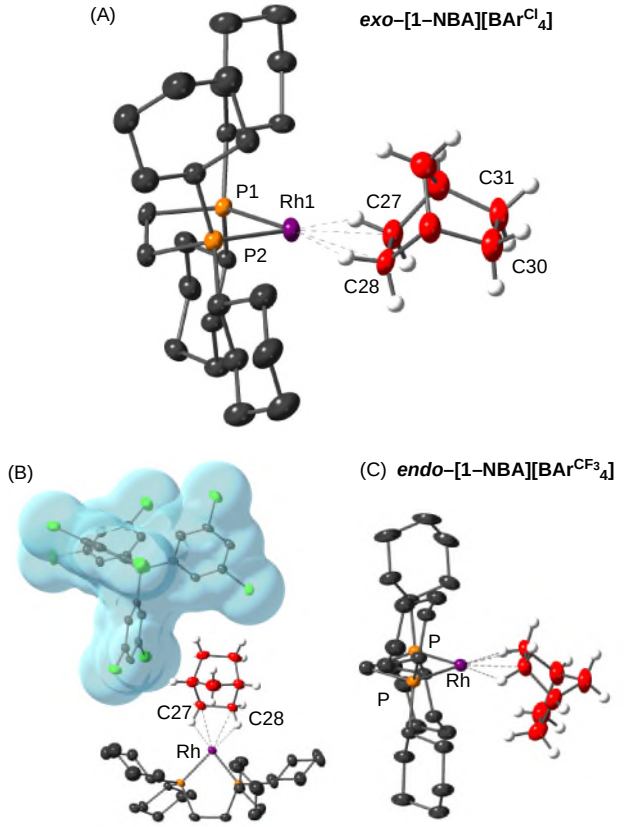

Figure 7. (A) Solid-state structures of the cations in ***exo*–[1-NBA][BAr$^{Cl}_{4}$]**. Displacement ellipsoids are shown at 50% probability level. Hydrogen atoms excepting those on the alkane fragment omitted for clarity. Selected bond lengths (Å): Rh1-P1 2.2095(11), Rh1-P2 2.2059(12), Rh1-C27 2.387(5), Rh1-C28 2.378(5), C27-C28 1.561(7), C30-C31 1.548(9). (B) Relationship between the **[1–NBA]$^+$** cation and the proximal [BAr$^{Cl}_{4}$]$^-$ anion (van der Waals surface shown). (C) Molecular structure of the cation in **[1–NBA][BAr$^{CF_3}_{4}$]** demonstrating the endo–coordination motif of the cation.[24]

The hydrogen atoms associated with C27 and C28, i.e. the 3c–2e interactions, were located and their positions refined in the final model. These, and the relative orientation of the NBA fragment, show it is the *exo*–hydrogens of the NBA methylene groups C27/C28 that are interacting with Rh–center. This is in contrast to the identical cation in **[1–NBA][BAr$^{CF_3}_{4}$]** (Figure 7C) in which it is the *endo*–CH groups that interact with the

metal center.[24] This different orientation is thus due to the different anion packing in the solid–state. Closer inspection of the relationship between cation and proximal anion in **[1-NBA][BAr$^{Cl}_4$]** (Figure 7B) also reveals that the NBA bridge methylene group (C33) does not sit in the cleft of two aryl groups, as found in **[1–NBA][BAr$^{CF_3}_4$]** (Figure 1B), but instead the anion sits off to one side. This is consistent with the ^{1}H/^{13}C HETCOR studies that indicates that there are no ring–current shielded methylene groups in the solid–state.

Previous calculations on the isolated cation **[1–NBA]$^+$** have shown that the *exo*– and *endo*– forms are essentially isoenergetic and can be interconverted by a rocking motion (**TS$_{rock}$**, 9.1 kcal/mol, Figure 8A). However, when placed in the extended crystal environment periodic DFT calculations on **[1–NBA][BAr$^{CF_3}_4$]** revealed that the *endo*–isomer is now clearly favored by 9.7 kcal/mol, while the *exo*–isomer was kinetically accessible with a barrier to interconversion of 13.9 kcal/mol, albeit at very low equilibrium populations.[30] For **[1–NBA][BAr$^{Cl}_4$]** this situation is reversed. The most stable isomer is now ***exo*–[1–NBA][BAr$^{Cl}_4$]**, with the *endo*–isomer at 2.5 kcal/mol being kinetically accessible via **TS$_{rock}$** and a slightly smaller barrier of 10.1 kcal/mol (see Figure 8B and Supporting Materials). These calculations are fully consistent with observed, crystallographically determined structures, and highlight the importance of considering the extended environment rather than isolated metal–ligand complexes when discussing these solid–state structures. Interestingly, the *exo*–coordination of C–H···Rh interactions observed in **[1–NBA][BAr$^{Cl}_4$]** reflect the intermediate implicated in selective solid/gas H/D exchange processes in **[1–NBA][BAr$^{CF_3}_4$]**.[30]

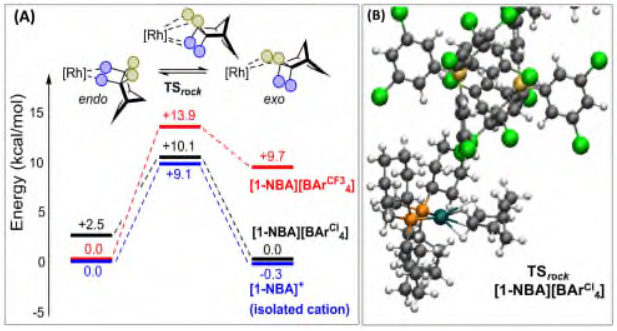

Figure 8. (A) Relative energies of *endo*– and *exo*–NBA isomers in **[1–NBA]$^+$** as a function of anion and their barriers for interconversion via TS$_{rock}$. **(B)** Detail of the structure of **TS$_{rock}$** computed in the solid-state for **[1-NBA][BAr$^{Cl}_4$]**. Method: [CP2K]PBE-D3/DZVP-MOLOPT-SR-GTH/GTH-PBE (cutoff 500 Ry).

2.4 Selectivity of the NBD hydrogenation and subsequent C–H Activation in the Solid-State. Reaction of **[1-NBD][BAr$^{CF_3}_4$]** with D_2 in a solid/gas reaction (5 minutes) proceeds with ~95% *endo* selectivity, forming ***endo,endo*–D$_4$–[1–NBA][BAr$^{CF_3}_4$]** as determined by GC–MS and ^{1}H/^{2}H NMR spectroscopy of the liberated NBA and single–crystal neutron diffraction.[30] When **[1-NBA][BAr$^{CF_3}_4$]** is exposed to D_2 (16 hours) C–H activation occurs at the remote, *exo*–C–H bond, to give ***exo*–D$_4$–[1–NBA][BAr$^{CF_3}_4$]**. No H/D exchange was observed at the *endo*-sites despite it being these that interact with the Rh center. This latter experiment shows that the *exo* sites are both accessible (Figure 8) and kinetically competent for C–H activation. That the D_4 isotopologue is selectively formed also demonstrates a fluxional process is occurring in the solid–state that brings both sets of *exo*–C–H bonds to the Rh–center. This was shown experimentally and computationally to be a low energy C_2 rotation of the NBA fragment in ***endo*–[1-NBA][BAr$^{CF_3}_4$]**. Interestingly, when [Rh(^{i}Bu$_2$PCH$_2$CH$_2$P^{i}Bu$_2$)($\eta^2\eta^2$-NBD)][BAr$^{CF_3}_4$] is exposed briefly to D_2, *endo*-D$_2$-*exo*-D$_2$-NBA results, the different selectivity demonstrating reorganization in the solid–state via an intermediate NBE complex.[26]

The selectivity of H_2 addition to **[1-NBD][BAr$^X_4$]** (X = Cl, F, H) was similarly studied. Longer reaction times (40 h) and powdering of precursor were employed due to the significantly slower rates of hydrogenation exhibited by these complexes relative to **[1-NBD][BAr$^{CF_3}_4$]**. For **[1-NBA][BAr$^{Cl}_4$]**, the ^{2}H NMR spectrum of the liberated alkane (vacuum transferred using CD_2Cl_2) shows deuterium incorporation in both the *endo*–(δ 1.16) and *exo*–sites (δ 1.46) [Lit. d_4–methanol: 1.21 and 1.52 respectively[64]]. Relative integrals, calibrated to the bridgehead methine resonance, from the corresponding ^{1}H NMR spectrum show deuterium incorporation at the *endo* positions to be ~90% and ~25% at the *exo* positions (Scheme 3). GC-MS indicated the major ion at *m*/*z* = 100.1185 which corresponds to **D$_4$–NBA** (calcd. $C_7H_8D_4$ = 100.1190). Additional ions were observed at *m*/*z* = 102.1310 (calcd. $C_7H_6D_6$ = 102.1315) and m/z = 104.1437 (calcd. $C_7H_4D_8$ = 104.1441) all with fragmentation patterns very similar to NBA, consistent with the incorporation of six and eight deuterium atoms respectively. These data are consistent with reductive deuteration of the alkenes to form **D$_4$–[1-NBA][BAr$^{Cl}_4$]** and then subsequent C–H activation of the alkane in a solid/gas reaction. Similar NMR and mass spectral data were obtained for the liberated alkane obtained via reaction of powdered **[1-NBD][BAr$^F_4$]** with D_2. In contrast GC–MS of NBA liberated from the analogous reaction with **[1-NBD][BAr$^H_4$]**, features a single ion at *m*/*z* = 100.1181 (calcd. $C_7H_8D_4$ = 100.1190) consistent with deuteration of the double bonds only and that no H/D exchange is occurring. This is consistent with the poor stability of **[1-NBA][BAr$^H_4$]** relative to **[1-NBA][BAr$^{Cl}_4$]** and **[1-NBA][BAr$^F_4$]**. The relative integrals in the ^{1}H NMR spectrum of the liberated NBA shows the deuterium addition is selective (~90%) for the *endo*–faces.

Scheme 3. D$_2$ addition to [1-NBD][BAr$^X_4$]. The signal at *m*/*z* = 1 lower than the parent ion (i.e. m/z = 99.1) reflects the fragmentation pattern of NBA: NBA–[H]$^•$.

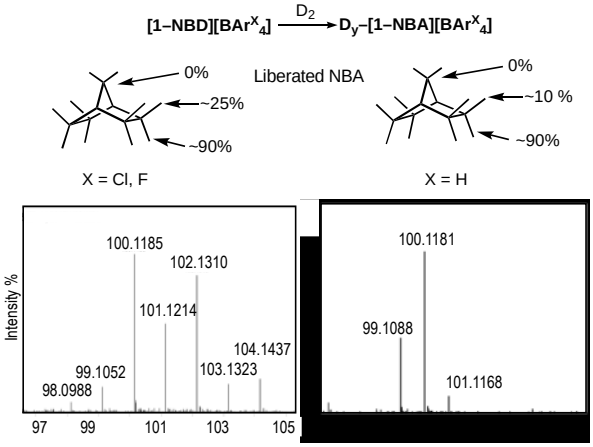

The slow hydrogenation and poor stability of all the resulting σ-alkane complexes reported here meant that delineation of the selectivities of the initial hydrogenation and the H/D exchange reactions was not possible, unlike for **[1–NBA][BAr$^{CF_3}_4$]**. Nev-

ertheless the observation of 90% *endo*, 25% *exo* deuterium incorporation for **[1-NBD][BAr$^{F}_4$]** and **[1-NBD][BAr$^{Cl}_4$]** suggests H/D exchange occurs at the alkane as well as D_2 addition to the alkene (which would only produce 100% total *endo*/*exo* D–incorporation). Further evidence for C–H activation at the bound alkane ligand in the solid–state comes from addition of D_2 to **[1-NBD][BAr$^{Cl}_4$]** or **[1-NBD][BAr$^{F}_4$]** in CD_2Cl_2 solution, where the NBA ligand is lost to solvent coordination,[24,26] and only deuteration of the double bonds is observed.

2.5 Catalytic 1-butene isomerization. We have previously shown[31] **[1-NBA][BAr$^{CF3}_4$]** to be effective in solid-state molecular organometallic catalysis (SMOM-cat) for the isomerization of 1–butene to a mixture of *cis*-and *trans*-2-butene at 298 K and 1 atm. Studies suggest catalysis is likely dominated by active species near to the surface of the crystal, although the NBA ligand is readily displaced by alkene in the whole crystal. In situ prepared **[1-NBA][BAr$^{X}_4$]** (X = Cl, F, H) enabled the effect of the anion on the catalytic isomerization of 1-butene to be studied. Catalysts were prepared by hydrogenation of ~2 mg of finely powdered NBD–precursors in an NMR tube for 1 hour to form the corresponding NBA–alkane complexes in the proportions shown in Figure 4B. These in situ prepared catalysts were then exposed to 1–butene gas and the progress of the resulting solid/gas isomerization catalysis followed by gas–phase NMR spectroscopy and gas chromatography (Figure 9A). As shown previously **[1-NBA][BAr$^{CF3}_4$]** is a very effective catalyst, and the first measured point (1 minute) shows that the thermodynamic equilibrium[65] between 1–butene and 2–butene is almost reached at 94% conversion (ToN = 54, $ToF_{(min)}$ = 3170 hr^{-1}). Complexes **[1-NBA][BAr$^{Cl}_4$]** and **[1-NBA][BAr$^{F}_4$]** were both found to be active catalysis, but slower than **[1-NBA][BAr$^{CF3}_4$]**. These systems are also active on recharging with 1–butene (Supporting Materials). These recharging experiments showed slightly reduced ToF which we have previously commented upon as being due to the formation of **[1-butadiene]$^+$** – by a transfer dehydrogenation of 1–butene – which is a poorer catalyst.[31]

The relative rates of isomerization track the relative proportions of alkane complex formed after 1 hour of hydrogenation (Figure 4B). Figure 9B compares relative conversion after 2 minutes and 60 minutes, and **[1-NBA][BAr$^{Cl}_4$]** is faster than **[1-NBA][BAr$^{F}_4$]**, consistent with the higher proportion of NBA alkane complex present. All eventually reach close to the thermodynamic equilibrium for 1–butene/2–butene ensemble.[65] Precatalyst **[1-NBD][BAr$^{H}_4$]** is essentially inactive post activation with H_2, as the alkane complex is not persistent. Without H_2 activation all the NBD precatalysts are inactive for isomerization. These observations regarding catalyst activity and active–site structure are similar to those made by Bianchini and co–workers on the role of active–site isolation in solid/gas ethene hydrogenation using $[Ir(triphos)(H)_2(C_2H_4)][X]$.[37] When X = $[BAr^{H}_4]^-$ dimerization occurs at temperatures above 70ºC to form a much less active hydride bridged species. In contrast, with the much larger polyoxometalate $[PW_{12}O_{40}]^{3-}$ dimerization is avoided as the active–sites are isolated.

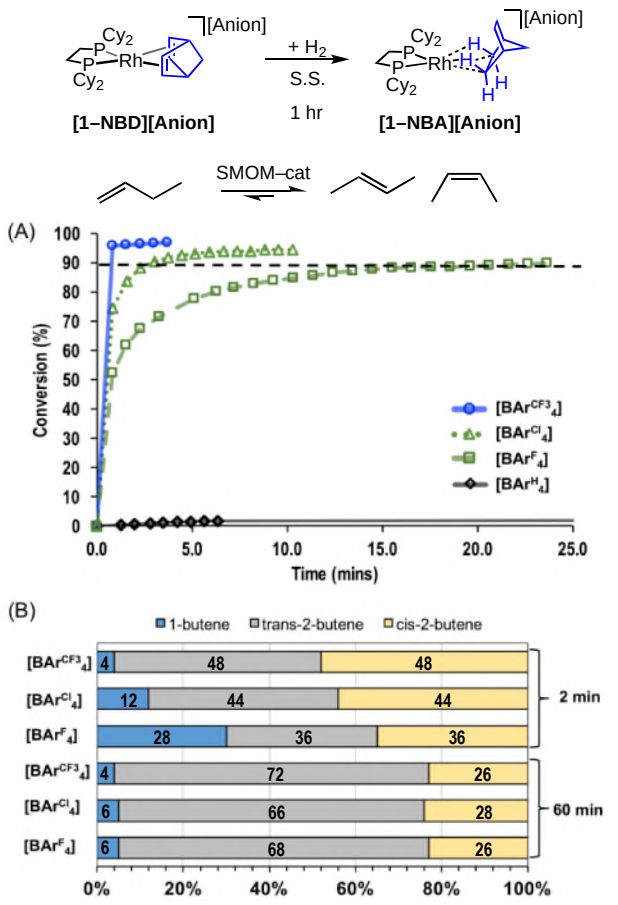

Figure 9. (A) Comparison of catalysts in the isomerization of 1-butene to 2-butene as measured by gas phase ^{1}H NMR spectroscopy. All catalysts = ~2.0 mg finely powdered sample. Complexes **[1-NBA][BAr$^{X}_4$]** (X = Cl, F, H) were prepared in situ. 1-Butene = 1 atm (86 μmol at 298 K). Dashed line indicates 90% conversion. (B) Relative ratio of 1–butene, *trans*–2–butene and *cis*–2–butene as measured by GC.

Monitoring the 2–butene *cis*/*trans* ratio over time shows at the early stages of catalysis (2 minutes) a *cis*/*trans* ratio of ~1:1 for all three active catalysts (Figure 9B). When left for an extended time (60 minutes) the ratio changes to be very close to the thermodynamic position of ~1:3 at 298 K. This demonstrates that *cis* 2–butene is the kinetic product, and we suggest this is driven by the relative stabilities of *cis* and *trans* isomers when bound to the Rh–catalyst.[31] The observed resting state in the **[1-NBA][BAr$^{CF3}_4$]** system is the *cis*–isomer of **[1–(2–butene)][BAr$^{CF3}_4$]**, an observation supported by periodic DFT calculations that show the *cis*–coordinated isomer to be 11.4 kcal mol^{-1} more stable than the *trans*, reflecting the microenvironment imposed by the crystalline lattice, and 5.7 kcal/mol more stable than the 1–butene complex. The initial 1:1 ratio observed here and then equilibration to the thermodynamic limit suggest reversible binding of the isomers of 2–butene post isomerization; and that compared with the *cis*–2–butene resting state, isomerization and then loss of *trans*–2–butene at the metal center presents the overall the highest energy span within the system. Similar selectivity for *cis*– over *trans*–2-butene have been noted for Pt–nanoparticle catalysts[66] and suggested to be due to the increased stability of the surface–bound *cis*–isomer. Homogeneous[67] and surface supported organometallic systems (under

propene metathesis conditions) have also been shown to show selectively at early stage of catalysis for *cis*–butene.[68]

3 Conclusions. The interplay between reactive cationic metal center and weakly coordinating anion is a well–established way of tuning structure, reactivity and stability in homogenous organometallic catalytic systems. We have extended this concept to solid-state molecular organoMetallic systems (SMOM), by using solid/gas reactivity to synthesize, sometimes transient, sigma–alkane complexes and then benchmarked their reactivity for alkene isomerization. Although, of the anions studied, only $[BAr^{CF_3}{}_4]^-$ affords indefinitely stable sigma–alkane complexes, there is a strong correlation between the lifetime of the complexes and catalytic activity in 1–butene double bond isomerization. The relative rates of hydrogenation of the NBD precursors are less straightforward to rationalize, but it is clear that the $–CF_3$ groups on the $[BAr^{CF_3}{}_4]$ anion play a significant role in both facilitating the movement of H_2 through the essentially non–porous crystalline framework and stabilizing the lattice towards collapse. More generally, the ability for the anion framework to control the spatial orientation and stereochemistry of the bonding mode of the alkane ligand with the metal center, e.g. ***exo*–[1–NBA][BAr$^{Cl}_4$]**, suggests future opportunities to harness the local microenvironment in SMOM systems to control selectivity in catalytic processes.[61] This is similar to that recently reported in catalysts encapsulated in metal–organic–frameworks that also offer a local spatial environment that promotes selectivity for one pathway over another.[69]

ASSOCIATED CONTENT

Supporting Information

The Supporting Information is available free of charge on the ACS Publications website.
Experimental and characterization details, including NMR spectroscopic data, X-ray crystallographic data, and computational details (PDF)
X-ray crystallographic data (CIF)
Cartesian coordinates for calculated structures (XYZ)

AUTHOR INFORMATION

*E-mail for A.S.W.: andrew.weller@chem.ox.ac.uk.

*E-mail for S.A.M.: s.a.macgregor@hw.ac.uk.

The authors declare no competing financial interests.

ACKNOWLEDGMENT

SCG Chemicals Co., Ltd, Thailand (A.S.W.) and the EPSRC (A.S.W., S.A.M.; EP/M024210, EP/K035908, EP/K035681) for funding. This work used the ARCHER UK National Supercomputing Service (http://www.archer.ac.uk).

REFERENCES

(1) *Activation and Functionalization of C-H Bonds*; Goldberg, K. I.; Goldman, A. S., Eds.; American Chemical Society, 2004.

(2) Choi, J.; MacArthur, A. H. R.; Brookhart, M.; Goldman, A. S. Dehydrogenation and Related Reactions Catalyzed by Iridium Pincer Complexes, *Chem. Rev.* **2011,** *111*, 1761-1779.

(3) Goldberg, K. I.; Goldman, A. S. Large-Scale Selective Functionalization of Alkanes, *Acc. Chem. Res.* **2017,** *50*, 620-626.

(4) Crabtree, R. H.; Lei, A. Introduction: CH Activation, *Chem. Rev.* **2017,** *117*, 8481-8482 and references therein.

(5) Kubas, G. J. *Metal Dihydrogen and σ-Bond Complexes*; Kluwer Academic: New York, 2001.

(6) Arndtsen, B. A.; Bergman, R. G.; Mobley, T. A.; Peterson, T. H. Selective Intermolecular Carbon-Hydrogen Bond Activation by Synthetic Metal Complexes in Homogeneous Solution, *Acc. Chem. Res.* **1995,** *28*, 154-162.

(7) Crabtree, R. H. Alkane C-H activation and functionalization with homogeneous transition metal catalysts: a century of progress-a new millennium in prospect, *J. Chem. Soc., Dalton Trans.* **2001**, 2437-2450.

(8) Labinger, J. A.; Bercaw, J. E. Understanding and exploiting C-H bond activation, *Nature* **2002,** *417*, 507-514.

(9) Cobar, E. A.; Khaliullin, R. Z.; Bergman, R. G.; Head-Gordon, M. Theoretical study of the rhenium–alkane interaction in transition metal–alkane σ-complexes, *Proc. Natl. Acad. Sci. U.S.A.* **2007,** *104*, 6963-6968.

(10) Balcells, D.; Clot, E.; Eisenstein, O. C—H Bond Activation in Transition Metal Species from a Computational Perspective, *Chem. Rev.* **2010,** *110*, 749-823.

(11) Weller, A. S.; Chadwick, F. M.; McKay, A. I. Chapter Five - Transition Metal Alkane-Sigma Complexes: Synthesis, Characterization, and Reactivity, *Adv. Organomet. Chem.* **2016,** *66*, 223-276.

(12) Ball, G. E.; Brookes, C. M.; Cowan, A. J.; Darwish, T. A.; George, M. W.; Kawanami, H. K.; Portius, P.; Rourke, J. P. A delicate balance of complexation vs. activation of alkanes interacting with [Re(Cp)(CO)(PF_3)] studied with NMR and time-resolved IR spectroscopy, *Proc. Natl. Acad. Sci. U.S.A.* **2007,** *104*, 6927-6932.

(13) Hall, C.; Perutz, R. N. Transition Metal Alkane Complexes†, *Chem. Rev.* **1996,** *96*, 3125-3146.

(14) Cowan, A. J.; Portius, P.; Kawanami, H. K.; Jina, O. S.; Grills, D. C.; Sun, X.-Z.; McMaster, J.; George, M. W. Time-resolved infrared (TRIR) study on the formation and reactivity of organometallic methane and ethane complexes in room temperature solution, *Proc. Natl. Acad. Sci. U.S.A.* **2007,** *104*, 6933-6938.

(15) Geftakis, S.; Ball, G. E. Direct Observation of a Transition Metal Alkane Complex, $CpRe(CO)_2$(cyclopentane), Using NMR Spectroscopy, *J. Am. Chem. Soc.* **1998,** *120*, 9953-9954.

(16) Lawes, D. J.; Geftakis, S.; Ball, G. E. Insight into Binding of Alkanes to Transition Metals from NMR Spectroscopy of Isomeric Pentane and Isotopically Labeled Alkane Complexes, *J. Am. Chem. Soc.* **2005,** *127*, 4134-4135.

(17) Lawes, D. J.; Darwish, T. A.; Clark, T.; Harper, J. B.; Ball, G. E. A Rhenium–Cyclohexane Complex with Preferential Binding of Axial C-H Bonds: A Probe into the Relative Ability of C-H, C-D, and C-C Bonds as Hyperconjugative Electron Donors?, *Angew. Chem. Int. Ed.* **2006,** *45*, 4486-4490.

(18) Calladine, J. A.; Torres, O.; Anstey, M.; Ball, G. E.; Bergman, R. G.; Curley, J.; Duckett, S. B.; George, M. W.; Gilson, A. I.; Lawes, D. J.et al. Photoinduced N_2 loss as a route to long-lived organometallic alkane complexes: A time-resolved IR and NMR study, *Chem. Sci.* **2010,** *1*, 622-630.

(19) Bernskoetter, W. H.; Schauer, C. K.; Goldberg, K. I.; Brookhart, M. Characterization of a Rhodium(I) σ-Methane Complex in Solution, *Science* **2009,** *326*, 553-556.

(20) Walter, M. D.; White, P. S.; Schauer, C. K.; Brookhart, M. Stability and Dynamic Processes in 16VE Iridium(III) Ethyl Hydride and Rhodium(I) σ-Ethane Complexes: Experimental and Computational Studies, *J. Am. Chem. Soc.* **2013,** *135*, 15933-15947.

(21) Yau, H. M.; McKay, A. I.; Hesse, H.; Xu, R.; He, M.; Holt, C. E.; Ball, G. E. Observation of Cationic Transition Metal–Alkane Complexes with Moderate Stability in Hydrofluorocarbon Solution, *J. Am. Chem. Soc.* **2016,** *138*, 281-288.

(22) Pike, S. D.; Weller, A. S. Organometallic synthesis, reactivity and catalysis in the solid state using well-defined single-site species, *Phil. Trans. R. Soc. A* **2015,** *373*, 20140187.

(23) Vittal, J. J.; Quah, H. S. Engineering solid state structural transformations of metal complexes, *Coord. Chem. Rev.* **2017,** *342*, 1-18.

(24) Pike, S. D.; Chadwick, F. M.; Rees, N. H.; Scott, M. P.; Weller, A. S.; Krämer, T.; Macgregor, S. A. Solid-State Synthesis and

Characterization of σ-Alkane Complexes, $[Rh(L_2)(\eta^2,\eta^2\text{-}C_7H_{12})][BAr^F{}_4]$ (L2 = Bidentate Chelating Phosphine), *J. Am. Chem. Soc.* **2015,** *137*, 820-833.

(25) McKay, A. I.; Krämer, T.; Rees, N. H.; Thompson, A. L.; Christensen, K. E.; Macgregor, S. A.; Weller, A. S. Formation of a σ-alkane Complex and a Molecular Rearrangement in the Solid-State: $[Rh(Cyp_2PCH_2CH_2PCyp_2)(\eta^2{:}\eta^2\text{-}C_7H_{12})][BAr^F{}_4]$, *Organometallics* **2017,** *36*, 22-25.

(26) Pike, S. D.; Thompson, A. L.; Algarra, A. G.; Apperley, D. C.; Macgregor, S. A.; Weller, A. S. Synthesis and Characterization of a Rhodium(I) σ-Alkane Complex in the Solid State, *Science* **2012,** *337*, 1648-1651.

(27) Inokuma, Y.; Kawano, M.; Fujita, M. Crystalline molecular flasks, *Nat. Chem.* **2011,** *3*, 349-358.

(28) Copéret, C.; Comas-Vives, A.; Conley, M. P.; Estes, D. P.; Fedorov, A.; Mougel, V.; Nagae, H.; Núñez-Zarur, F.; Zhizhko, P. A. Surface Organometallic and Coordination Chemistry toward Single-Site Heterogeneous Catalysts: Strategies, Methods, Structures, and Activities, *Chem. Rev.* **2016,** *116*, 323-421.

(29) Thomas, J. M.; Thomas, W. J. *Principles and Practice of Heterogeneous Catalysis, 2nd Edition*; Wiley-VCH: Weinheim, 2015.

(30) Chadwick, F. M.; Krämer, T.; Gutmann, T.; Rees, N. H.; Thompson, A. L.; Edwards, A. J.; Buntkowsky, G.; Macgregor, S. A.; Weller, A. S. Selective C–H Activation at a Molecular Rhodium Sigma-Alkane Complex by Solid/Gas Single-Crystal to Single-Crystal H/D Exchange, *J. Am. Chem. Soc.* **2016,** *138*, 13369-13378.

(31) Chadwick, F. M.; McKay, A. I.; Martinez-Martinez, A. J.; Rees, N. H.; Kramer, T.; Macgregor, S. A.; Weller, A. S. Solid-state molecular organometallic chemistry. Single-crystal to single-crystal reactivity and catalysis with light hydrocarbon substrates, *Chem. Sci.* **2017,** *8*, 6014-6029.

(32) Macchioni, A. Ion Pairing in Transition-Metal Organometallic Chemistry, *Chem. Rev.* **2005,** *105*, 2039-2074.

(33) Riddlestone, I. M.; Kraft, A.; Schaefer, J.; Krossing, I. Taming the Cationic Beast: Novel Developments in the Synthesis and Application of Weakly Coordinating Anions *Angew. Chem. Int. Ed.*, DOI: 10.1002/anie.201710782.

(34) Siedle, A. R.; Newmark, R. A.; Brown-Wensley, K. A.; Skarjune, R. P.; Haddad, L. C.; Hodgson, K. O.; Roe, A. L. Solid-state organometallic chemistry of molecular metal oxide clusters: carbon-hydrogen activation by an iridium polyoxometalate, *Organometallics* **1988,** *7*, 2078-2079.

(35) Siedle, A. R.; Newmark, R. A.; Sahyun, M. R. V.; Lyon, P. A.; Hunt, S. L.; Skarjune, R. P. Solid-state chemistry of molecular metal oxide clusters. Multiple, sequential carbon-hydrogen activation processes in the hydrogenation of coordinated cyclooctene. Lattice mobility of small organic molecules, *J. Am. Chem. Soc.* **1989,** *111*, 8346-8350.

(36) Bianchini, C.; Mealli, C.; Peruzzini, M.; Zanobini, F. Reversible uptake of hydrogen and nitrogen at cobalt in the solid state. Influence of the counter anion on the formation of classical dihydride vs. nonclassical .eta.2-dihydrogen forms of $[(PP_3)CoH_2]^+$, *J. Am. Chem. Soc.* **1992,** *114*, 5905-5906.

(37) Bianchini, C.; Farnetti, E.; Graziani, M.; Kaspar, J.; Vizza, F. Molecular solid-state organometallic chemistry of tripodal (polyphosphine)metal complexes. Catalytic hydrogenation of ethylene at iridium, *J. Am. Chem. Soc.* **1993,** *115*, 1753-1759.

(38) Pike, S. D.; Weller, A. S. C-Cl activation of the weakly coordinating anion $[B(3,5\text{-}Cl_2C_6H_3)_4]^-$ at a Rh(I) centre in solution and the solid-state, *Dalton Trans.* **2013,** *42*, 12832-12835.

(39) Spek, A. L. Structure validation in chemical crystallography, *Acta Cryst. D* **2009,** *65*, 148-155.

(40) Alvarez, S. A cartography of the van der Waals territories, *Dalton Trans.* **2013,** *42*, 8617-8636.

(41) Thalladi, V. R.; Weiss, H.-C.; Bläser, D.; Boese, R.; Nangia, A.; Desiraju, G. R. C−H···F Interactions in the Crystal Structures of Some Fluorobenzenes, *J. Am. Chem. Soc.* **1998,** *120*, 8702-8710.

(42) Desiraju, G. R.; Parthasarathy, R. The nature of halogen.cntdot..cntdot..cntdot.halogen interactions: are short halogen contacts due to specific attractive forces or due to close packing of nonspherical atoms?, *J. Am. Chem. Soc.* **1989,** *111*, 8725-8726.

(43) Boese, R.; Kirchner, M. T.; Dunitz, J. D.; Filippini, G.; Gavezzotti, A. Solid-State Behaviour of the Dichlorobenzenes: Actual, Semi-Virtual and Virtual Crystallography, *Helv. Chim. Acta* **2001,** *84*, 1561-1577.

(44) Dunitz, J. D.; Schweizer, W. B. Molecular Pair Analysis: C-H···F Interactions in the Crystal Structure of Fluorobenzene? And Related Matters, *Chem. Eur. J.* **2006,** *12*, 6804-6815.

(45) Cavallo, G.; Metrangolo, P.; Milani, R.; Pilati, T.; Priimagi, A.; Resnati, G.; Terraneo, G. The Halogen Bond, *Chem. Rev.* **2016,** *116*, 2478-2601.

(46) Desiraju, G. R. Crystal Gazing: Structure Prediction and Polymorphism, *Science* **1997,** *278*, 404-405.

(47) The bridgehead carbons are coincidental.

(48) At room temperature dichloromethane solutions of **[1-$BAr^{Cl}{}_4$]** undergo C-Cl activation of the anion to afford $[RhCl(Cy_2PCH_2CH_2PCy_2)\{C_6H_3Cl(BAr^{Cl}{}_3)\}]_2$ which precipitates from solution. Hence, the data presented in Figures 4 and 5 represents the minimum amount of **[1-NBA][$BAr^{Cl}{}_4$]** formed.

(49) An increased pressure of hydrogen was employed to accelerate the hydrogenation of the alkene.

(50) See Supporting Information.

(51) Albano, P.; Aresta, M.; Manassero, M. Interaction of carbon dioxide with coordinatively unsaturated rhodium(I) complexes with the ligand 1,2-bis(diphenylphosphino)ethane, *Inorg. Chem.* **1980,** *19*, 1069-1072.

(52) Longato, B.; Pilloni, G.; Graziani, R.; Casellato, U. Heteropolymetallic complexes of 1,1′-bis(diphenylphosphino)ferrocene (dppf): VI. Synthesis and crystal structure of $[Rh(dppf)(\eta^6\text{-}C_6H_5B(C_6H_5)_3]$, *J. Organomet. Chem.* **1991,** *407*, 369-376.

(53) Shestakova, E. P.; Varshavsky, Y. S.; Khrustalev, V. N.; Podkorytov, I. S. A novel reaction producing the rhodium(I) complexes with π-coordinated tetraphenylborate anion, $(\pi\text{-}PhBPh_3)^-$. X-ray study of $[Rh(PPh_3)_2(\pi\text{-}PhBPh_3)]$, *J. Organomet. Chem.* **2007,** *692*, 4297-4302.

(54) Grochowski, M. R.; Morris, J.; Brennessel, W. W.; Jones, W. D. C–CN Bond Activation of Benzonitrile with [Rh–I(dippe)]−, *Organometallics* **2011,** *30*, 5604-5610.

(55) Schrock, R. R.; Osborn, J. A. .pi.-Bonded complexes of the tetraphenylborate ion with rhodium(I) and iridium(I), *Inorg. Chem.* **1970,** *9*, 2339-2343.

(56) Li, X.; Baldamus, J.; Nishiura, M.; Tardif, O.; Hou, Z. Cationic Rare-Earth Polyhydrido Complexes: Synthesis, Structure, and Catalytic Activity for the cis-1,4-Selective Polymerization of 1,3-Cyclohexadiene, *Angew. Chem. Int. Ed.* **2006,** *45*, 8184-8188.

(57) Bouwkamp, M. W.; Budzelaar, P. H. M.; Gercama, J.; Del Hierro Morales, I.; de Wolf, J.; Meetsma, A.; Troyanov, S. I.; Teuben, J. H.; Hessen, B. Naked $(C_5Me_5)_2M$ Cations (M = Sc, Ti, and V) and Their Fluoroarene Complexes, *J. Am. Chem. Soc.* **2005,** *127*, 14310-14319.

(58) Smart, K. A.; Grellier, M.; Coppel, Y.; Vendier, L.; Mason, S. A.; Capelli, S. C.; Albinati, A.; Montiel-Palma, V.; Muñoz-Hernández, M. A.; Sabo-Etienne, S. Nature of Si–H Interactions in a Series of Ruthenium Silazane Complexes Using Multinuclear Solid-State NMR and Neutron Diffraction, *Inorg. Chem.* **2014,** *53*, 1156-1165.

(59) Chadwick, F. M.; Rees, N. H.; Weller, A. S.; Krämer, T.; Iannuzzi, M.; Macgregor, S. A. A Rhodium–Pentane Sigma-Alkane Complex: Characterization in the Solid State by Experimental and Computational Techniques, *Angew. Chem. Int. Ed.* **2016,** *55*, 3677-3681.

(60) The solvent accessible voids in **[1-NBD][$BAr^{CF3}{}_4$]** were found to account for 0.8% of the total unit cell volume.

(61) Huang, Z.; White, P. S.; Brookhart, M. Ligand exchanges and selective catalytic hydrogenation in molecular single crystals, *Nature* **2010,** *465*, 598-601.

(62) Vitorica-Yrezabal, I. J.; Minguez Espallargas, G.; Soleimannejad, J.; Florence, A. J.; Fletcher, A. J.; Brammer, L. Chemical transformations of a crystalline coordination polymer: a multi-stage solid-vapour reaction manifold, *Chem. Sci.* **2013,** *4*, 696-708.

(63) Thallapally, P. K.; Peter McGrail, B.; Dalgarno, S. J.; Schaef, H. T.; Tian, J.; Atwood, J. L. Gas-induced transformation and expansion of a non-porous organic solid, *Nat. Mater.* **2008,** *7*, 146.

(64) Nguyen, B.; Brown, J. M. Stereoselectivity in the Rhodium-Catalysed Reductions of Non-Conjugated Dienes, *Adv. Synth. Catal.* **2009,** *351*, 1333-1343.

(65) Kapteijn, F.; van der Steen, A. J.; Mol, J. C. Thermodynamics of the geometrical isomerization of 2-butene and 2-pentene, *J. Chem. Thermodyn.* **1983,** *15*, 137-146.

(66) Lee, I.; Delbecq, F.; Morales, R.; Albiter, M. A.; Zaera, F. Tuning selectivity in catalysis by controlling particle shape, *Nat. Mater.* **2009,** *8*, 132.

(67) Tolman, C. A. Chemistry of tetrakis(triethyl phosphite)nickel hydride, $HNi[P(OEt)_3]^{4+}$. IV. Mechanism of olefin isomerization, *J. Am. Chem. Soc.* **1972,** *94*, 2994-2999.

(68) Salameh, A.; Baudouin, A.; Soulivong, D.; Boehm, V.; Roeper, M.; Basset, J.-M.; Copéret, C. CH_3-ReO_3 on γ-Al_2O_3: Activity, selectivity, active site and deactivation in olefin metathesis, *J. Catal.* **2008,** *253*, 180-190.

(69) Grigoropoulos, A.; McKay, A. I.; Katsoulidis, A. P.; Davies, R. P.; Haynes, A.; Brammer, L.; Xiao, J.; Weller, A. S.; Rosseinsky, M. J. Encapsulation of Crabtree's Catalyst in Sulfonated MIL-101(Cr): Enhancement of Stability and Selectivity between Competing Reaction Pathways by the MOF Chemical Microenvironment, *Angew. Chem. Int. Ed.*, **2018**, *57*, 4532-4539.

Solid–state Molecular OrganoMetalic Chemistry (SMOM)

Anion microenvironment determines stability & binding selectivity of σ–alkane complexes

